ACS APPLIED MATERIALS & INTERFACES

Research Article

www.acsami.org

Cu(In,Ga)(S,Se)$_2$ Thin Film Solar Cell with 10.7% Conversion Efficiency Obtained by Selenization of the Na-Doped Spray-Pyrolyzed Sulfide Precursor Film

Wilman Septina,[†] Masaaki Kurihara,[‡] Shigeru Ikeda,*[,†] Yasuhiro Nakajima,[‡] Toshiyuki Hirano,[‡] Yoshihito Kawasaki,[†] Takashi Harada,[†] and Michio Matsumura[†]

[†]Research Center for Solar Energy Chemistry, Osaka University 1-3 Machikaneyama, Toyonaka, Osaka 560-8531, Japan

[‡]Renewable Energy Material Development Group, Energy & Environment R&D Center, Corporate Research & Development, Asahi Kasei Corporation 1-3-1, Yakoh, Kawasaki-ku, Kawasaki, Kanagawa 210-0863, Japan

Supporting Information

ABSTRACT: Selenium-rich Cu(In,Ga)(S,Se)$_2$ (CIGSSe) thin films on an Mo-coated soda-lime glass substrate were fabricated by spray pyrolysis of an aqueous precursor solution containing $Cu(NO_3)_2$, $In(NO_3)_3$, $Ga(NO_3)_3$, and thiourea followed by selenization at 560 °C for 10 min. We studied the effects of intentional sodium addition on the structural and morphological properties of the fabricated CIGSSe films by dissolving $NaNO_3$ in the aqueous precursor solution. The addition of sodium was found to affect the morphology of the final CIGSSe film: the film had denser morphology than that of the CIGSSe film obtained without addition of $NaNO_3$. Photoelectrochemical measurements also revealed that the acceptor density of the nondoped CIGSSe film was relatively high ($N_a = 7.2 \times 10^{17}$ cm^{-3}) and the addition of sodium led to a more favorable value for solar cell application ($N_a = 1.8 \times 10^{17}$ cm^{-3}). As a result, a solar cell based on the sodium-modified CIGSSe film exhibited maximum conversion efficiency of 8.8%, which was significantly higher than that of the cell based on nondoped CIGSSe (4.4%). In addition, by applying MgF_2 antireflection coating to the device, the maximum efficiency was further improved to 10.7%.

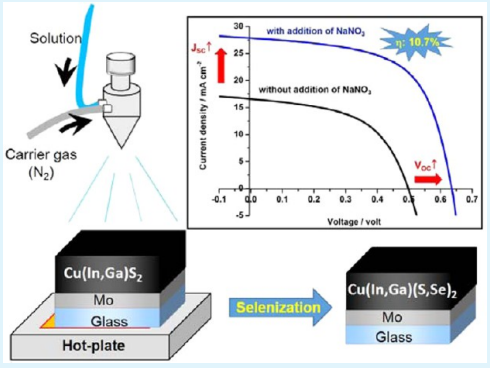

KEYWORDS: *Cu(In,Ga)(S,Se$_2$), spray pyrolysis, sodium addition, selenization, aqueous solution*

1. INTRODUCTION

Chalcopyrite Cu(In,Ga)Se$_2$ (CIGSe)-based solar cells have been intensively studied, and a relatively high conversion efficiency of 21.7% has been obtained by using a CIGSe film fabricated by coevaporation of its elements.[1] These cells are regarded as strong high-efficiency competitors to silicon-based solar cells, and their photovoltaic modules have been commercialized by several companies.[2−4] The emergence of CIGSe-based solar cell can be attributed due to their excellent intrinsic properties, such as adjustable band gap (1.0 to 1.7 eV) in a suitable range for optimal sunlight absorption, high absorption coefficient (more than 10^4 cm^{-1}) that allows the use of thin material to reduce material consumption, and tolerance to off-stoichiometric composition.[5] Furthermore, a polycrystalline structure was proven to be superior to a single crystalline structure, which allowed the versatility to use various methods to fabricate the materials.[6,7]

For a CIGSe-based thin film solar cell to be one of the dominant players in the solar cell market, reduction of the manufacturing cost of the absorber is an important issue. For this purpose, nonvacuum processes that use low-cost instruments and have high throughput are desirable. Spray pyrolysis is a method that satisfies those requirements because it is a low temperature process, can be used for large-area deposition, and is suitable for roll-to-roll production.[8−10] Moreover, composition of the film can be easily adjusted by controlling amounts of constituent metals in the precursor solution. Most of the reports on the spray pyrolysis-based chalcopyrite devices with appreciable conversion efficiencies involved spray pyrolysis of pure sulfide $CuInS_2$ or Cu(In,Ga)S$_2$ precursor film followed by sulfurization or selenization to produce their crystalline compounds or mixed sulfide-selenide compounds.[11,12] It is also possible to fabricate pure selenide $CuInSe_2$ or Cu(In,Ga)-Se$_2$ by spray pyrolysis.[13,14] However, for practical application, this approach is often avoided due to the toxicity of the volatile selenium source.

Another advantage of spray pyrolysis is that external dopants can be introduced to the film simply by adding dopant elements to the solution. For the CIGSe-based solar cell, this feature is advantageous especially to include Na (sodium) to the CIGSe. Several studies have shown enhancement of the photovoltaic properties of a CIGSe-based solar cell by adding

Received: November 4, 2014
Accepted: March 16, 2015
Published: March 16, 2015

DOI: 10.1021/am507684x
ACS Appl. Mater. Interfaces 2015, 7, 6472−6479

external sodium to the CIGSe films aside from that supplied from the soda-lime glass substrate.[15−18] Explanations for this beneficial effect are manifold,[15−20] such as enlargement of grain sizes of the film,[15,18] increase in conductivity of the material,[17,19] and compensation of point defects by O atoms facilitated by the presence of sodium components.[20] However, no conclusive mechanism of the actual role of sodium is given at present.

We attempted to fabricate a mixed sulfide-selenide Cu(In,Ga)$(S,Se)_2$ (CIGSSe) film by selenization of a spray-pyrolyzed Cu(In,Ga)S_2 (CIGS) precursor. For this purpose, we studied the effects of intentional sodium addition to the sulfide precursor film on the structural and electrical properties of the fabricated CIGSSe films in relation to their solar cell performance. The addition of sodium was performed by dissolving sodium nitrate ($NaNO_3$) in the precursor solution. A CIGSSe-based solar cell with conversion efficiency (η) of 10.7% after applying an antireflection coating to the device (8.8% without an antireflection coating) was achieved.

2. EXPERIMENTAL SECTION

2.1. Fabrication and Characterization of CIGSSe Films. A 6 cm^3 portion of aqueous solution containing 0.09 M $Cu(NO_3)_2$, 0.07 M $In(NO_3)_3$, 0.03 M $Ga(NO_3)_3$, and 0.8 M thiourea was sprayed using N_2 as a carrier gas. N_2 was used as the carrier gas instead of air in order to avoid a formation of appreciable MoO_2 layer on Mo-substrate. The molarity of the respective metal sources were chosen so that Cu-poor (Cu/(In+Ga) < 1) precursor film can be obtained. The excess thiourea (S/(Cu + In + Ga) = 4) compared to the stoichiometric ratio (S/(Cu + In + Ga) = 1) was used to avoid formation of a white precipitate which is likely to be a Cu-thiourea complex.[12] To study the effect of addition of sodium, $NaNO_3$ was dissolved in the precursor solution with an Na/(In + Ga) molar ratio of 0.3. Deposition of CIGS precursor films was performed on an Mo-coated glass substrate heated at 330−360 °C by using a hot plate. Distance between the substrate and the spray nozzle was fixed at 20 cm. The spray rate was fixed at 2 cm^3 min^{-1} by using a FUSO SEIKI Lumina STS-10SK and cycled two times. These experiments were conducted in the open atmosphere. Thus-obtained CIGS films were selenized in the presence of 5 mg elemental selenium powder in an evacuated borosilicate glass ampule at 560 °C for 10 min to obtain sulfur−selenium mixed CIGSSe films. Crystalline structures of the films were determined by using a Rigaku Mini Flex X-ray diffractometer (XRD, CuKα, Ni filter). Morphologies of the films were examined by using a Hitachi S-5000 FEG scanning electron microscope (SEM). Elemental compositions of the films were determined using a Hitachi TM3000 scanning electron microscope (SEM) equipped with a SwiftED3000 energy dispersive X-ray spectrometer (EDX).

Photoelectrochemical (PEC) measurements of CIGSSe films were carried out in 0.2 M $Eu(NO_3)_3$ electrolyte by using a conventional three-electrode cell.[21,22] A Pt wire and an Ag/AgCl electrode served as the counter electrode and reference electrode, respectively, and a Hokuto Denko HB-151 potentio-galvanostat was used to obtain photocurrent density−voltage (J−V) response. Photocurrent densities were measured using the lock-in technique to obtain external quantum efficiency (EQE) spectra.[22,23] Sample electrodes were illuminated with a monochromatic light of variable wavelength chopped at a frequency of 10 Hz. The number of incident photons was determined with an OPHIR Orion Laser power meter equipped with a photodiode.

2.2. Fabrication and Characterization of Solar Cells. For evaluation of solar cell properties of the CIGSSe films, they were processed to form an Al:ZnO/ZnO/CdS/CIGSSe/Mo/glass structure. A CdS buffer layer (~70 nm) was deposited by chemical bath deposition (CBD). Then an Al:ZnO/ZnO bilayer (~1 μm) was deposited on the top of the CdS layer by radio frequency (RF) magnetron sputtering. J−V characteristics of thus-obtained devices under simulated AM1.5 irradiation (100 mW cm^{-2}) were measured with a Bunkoh−Keiki CEP-015 photovoltaic measurement system.

Atomic concentrations of sodium in as-prepared CIGSSe-based devices were measured by using ULVAC-PHI ADEPT-1010 Quadrupole Dynamic secondary ion mass spectroscopy (SIMS). Resistivity profiles of the devices were obtained by a Bruker AXS NanoScope IV Dimension 3100 scanning probe microscope system equipped with a scanning spreading resistance microscopy (SSRM) module.

3. RESULTS AND DISCUSSION

Figure 1a shows typical XRD patterns of as-sprayed films fabricated from the precursor solution without and with addition of $NaNO_3$. In both films, weak diffraction peaks at 2θ of ~28.2°, 46.7°, and 56.1° were observed. Compared to (112), (220)/(204), and (312/116) reflections of chalcopyrite $CuInS_2$ (CIS), which give 2θ of 27.8°, 46.2°, and 55.1°, respectively (JCPDS 27-0159), they are slightly shifted toward high 2θ angle regions, indicating incorporation of Ga components in the chalcopyrite CIS crystalline lattice to form mixed crystal Cu(In,Ga)S_2 (CIGS). The XRD pattern of the CIGS precursor film obtained by adding $NaNO_3$ in the spray solution shows slightly strong peak intensities compared to those of the precursor film without addition of $NaNO_3$, though such weak and broad peaks suggest difficulty in applying the film as an absorber layer for thin-film solar cells in that shape. Upon selenization at 560 °C for 10 min, appreciable crystalline growth was observed in XRD patterns of both films, as shown in Figure 1b. Small shifts of diffraction peaks toward 2θ angle

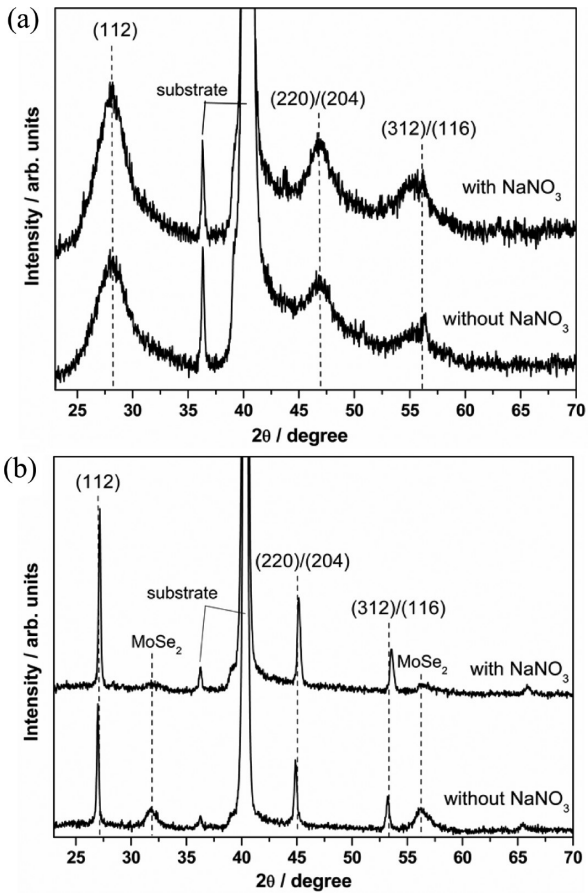

Figure 1. XRD patterns of (a) CIGS precursors obtained without and with addition of $NaNO_3$ to the precursor solution and (b) their respective selenized films.

DOI: 10.1021/am507684x
ACS Appl. Mater. Interfaces 2015, 7, 6472−6479

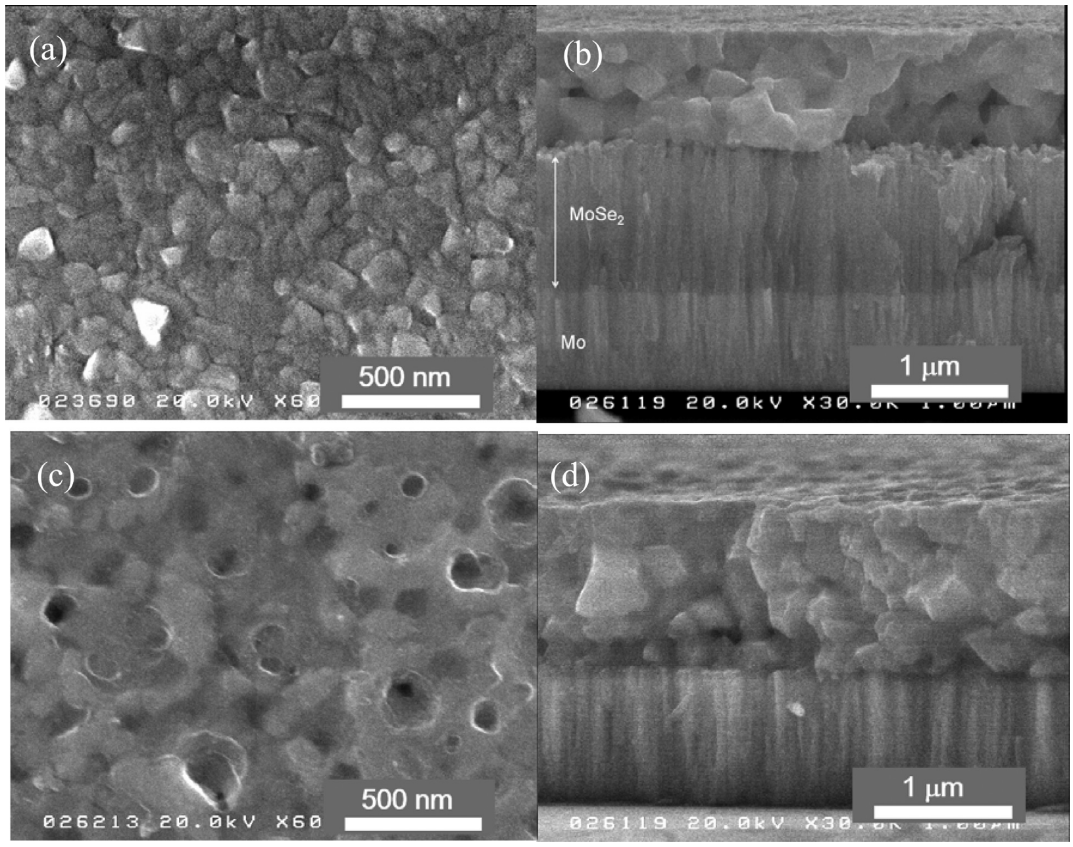

Figure 2. Typical (a, c) surface and (b, d) cross-sectional SEM images of CIGSSe films (a, b) without and (c, d) with addition of $NaNO_3$ to the precursor solution.

regions, that is, 27°, 45.1°, and 53.6° for (112), (220)/(204), and (312/116) reflections, respectively, were also observed, indicating partial replacement of sulfur with selenium to form $Cu(In,Ga)(S,Se)_2$ (CIGSSe) films. As confirmed by EDX analyses, thus-obtained CIGSSe films have Se/(S + Se) molar ratios of ~0.7 (Cu, 25 atom %; In, 18 atom %; Ga, 9 atom %; S, 15 atom %; Se, 34 atom %). The CIGSSe film obtained with addition of $NaNO_3$ (labeled CIGSSe(SNt)) had a relatively intense peak than that of the CIGSSe film obtained without addition of $NaNO_3$ (labeled CIGSSe(non)). In addition, the intensity of the peaks assigned to $MoSe_2$, due to partial selenization of the Mo substrate, were weaker in CIGSSe(SNt), indicating formation of a relatively thin $MoSe_2$ layer compared to that formed in the CIGSSe(non) sample.

Morphological properties of thus-obtained CIGSSe(non) and CIGSSe(SNt) films were investigated by SEM. As shown in Figure 2a, the CIGSSe(non) film was composed of granular grains of covering the entire surface without any observable voids. From the corresponding cross-section shown in Figure 2b, sizes of grains in the film were estimated to be ~200−400 nm. The CIGSSe(SNt) film exhibited a distinctively different grain structure. The grains seem to be interconnected to form a dense structure, as shown in Figure 2c. Such an interconnected structure was also obvious in its cross-section as shown in Figure 2d, while the sizes of grains were similar to the CIGSSe(non). Comparison of the cross-sectional images of these films also clearly indicated that CIGSSe(SNt) had a thicker layer (~1 μm) than that of the CIGSSe(non) (~800 nm). In fact, the as-sprayed film obtained with addition of $NaNO_3$ was also thicker than that obtained without addition of $NaNO_3$ (see Supporting Information Figure S1). In the above XRD results, this reflected stronger XRD peak intensities of the films obtained with addition of $NaNO_3$ before and after the selenization than those obtained without addition of $NaNO_3$. This implies that the addition of $NaNO_3$ somewhat improved the deposition efficiency during spray process, which likely to result in a dense morphology of the as-sprayed film. The dense structure would also be the main reason for formation of the significantly thinner $MoSe_2$ layer in the CIGSSe(SNt) sample due to suppression of the rapid diffusion of Se vapor through the intergrains to induce selenization of the Mo substrate.

A previous study showed that density of sodium in a typical CIGSe film is in the order of 10^{19}-10^{20} atoms cm^{-3}.[20] On the basis of the reported value of the lattice constant of CIGSe crystallite,[24] density of group III elements (In + Ga) in the CIGSe film can be calculated to be ~1.2×10^{22} atoms cm^{-3} by assuming that the film has a density similar to that of the corresponding single crystal. Hence, the Na/(In + Ga) atomic ratio is estimated to be in the order of 0.001−0.01. Since the Na/(In + Ga) ratio in the precursor solution with addition of $NaNO_3$ is 0.3, a considerable excess amount of sodium would be included in the sprayed film.

An interconnected morphology of the CIGSSe(SNt) film was typically observed in the presence of a liquid phase during the annealing process; such a liquid phase acted as a liquid flux to assist grain growth. In this system, presence of the Cu_xSe compound, which commonly acts as an efficient liquid flux during grain growth of CIGSe,[25,26] can be excluded because of the use of Cu-poor composition of our precursor solution. Thus, formation of the interconnected morphology is likely to be related to the presence of a large amount of sodium components in the film derived from $NaNO_3$ dissolved in the

DOI: 10.1021/am507684x
ACS Appl. Mater. Interfaces 2015, 7, 6472−6479

spray solution. Since the melting point of $NaNO_3$ (308 °C) is lower than the present selenization temperature, this can be fused during the spray deposition. Although most of $NaNO_3$ might be decomposed into a different compound(s) because the other metallic components mostly formed a CIGS compound during the spray deposition, such excess sodium components, therefore, would be present as sodium hydroxide (NaOH) by the reaction of atmospheric water vapor. The NaOH compound might also be a liquid-flux agent because its melting point (318 °C) is lower than the present spray-deposition and selenization temperatures. Apart from the grain morphology, another role of the sodium component is likely to be formation of sodium selenide (Na_2Se_x) during selenization. In accordance with some previous reports,[27,28] Na_2Se_x acts as an efficient Se source for the growth of CIGSSe grains, resulting in the formation of dense grains (see Figure 2c).

To estimate the acceptor densities of the CIGSSe(non) and CIGSSe(SNt) films, PEC measurements in 0.2 M $Eu(NO_3)_3$ electrolyte (pH 4) were performed. Figure 3a shows typical photocurrent−potential responses of the CIGSSe(non) and CIGSSe(SNt) films detected by using the lock-in technique. Both of the films showed appreciable photocurrents at potentials more negative than ca. 0.1 V vs Ag/AgCl, indicating formation of a Schottky junction between these p-type CIGSSe films and the electrolyte solution. At the fixed potential of −0.4 V vs Ag/AgCl, where an appreciable photocurrent due to band bending was produced, we measured the EQE spectra of these CIGSSe films, as shown in Figure 3b. The CIGSSe(non) film showed a significantly low EQE response, especially in a relatively long wavelength region. On the other hand, the CIGSSe(SNt) film appreciably enhanced the EQE response, indicating the achievement of appreciable improvement of film quality by just dissolving the $NaNO_3$ compound in the spray solution.

EQE is correlated with the width of the space charge region (W) according to the following equation:

$$\mathrm{EQE} = 1 - \exp(-\alpha W)$$

where α denotes the absorption coefficient. According to this equation, W can be estimated from the slope of $-\ln(1 - \mathrm{EQE})$ versus α plot, as shown in Figure 3c. When the α value of the films was estimated by using the value of the CIGSe film reported by Minoura et al.,[29] with the assumption of a linear shift with the band gap energy from 1.15 to 1.33 eV (see below), we could estimate W values of the CIGSSe films; these values were 30 and 60 nm for CIGSSe(non) and CIGSSe(SNt) films, respectively. By using W, the acceptor density (N_a) can be determined using the relation

$$W = ((2(E_{FB} - E)\varepsilon_0\varepsilon_r)/(qN_a))^{1/2}$$

where E_{FB}, E, ε_0, ε_r, and q denote flat band potential, applied bias potential, relative permittivity in the vacuum, relative permittivity of CIGSSe, and electric charge, respectively.[21] Assuming that E_{FB} can be estimated from its $J-V$ response onset (~0.1 V (vs Ag/AgCl), see Figure 3a) and applying the ε_r value of CIGSe (11.7),[30] N_a values of CIGSSe(non) and CIGSSe(SNt) films were calculated to be 7.2×10^{17} and 1.8×10^{17} cm^{-3}, respectively. In highly efficient (η > 15%) CIGSe-based solar cells, the absorber films generally have N_a values in the order of $10^{15}-10^{16}$ cm^{-3}.[31−33] To confirm the reliability of the N_a values estimated by the present method, we also estimated the N_a of coevaporated CIGSe film used in a high-efficient cell by similar method (see Supporting Information Figure S2 for the related figures).[34] The N_a of this film was estimated to be 6.5×10^{16} cm^{-3}, in which in reasonable value for absorber used in high-efficient cell. Hence, it is apparent that the CIGSSe films, especially the CIGSSe(non) film, have considerably high doping densities.

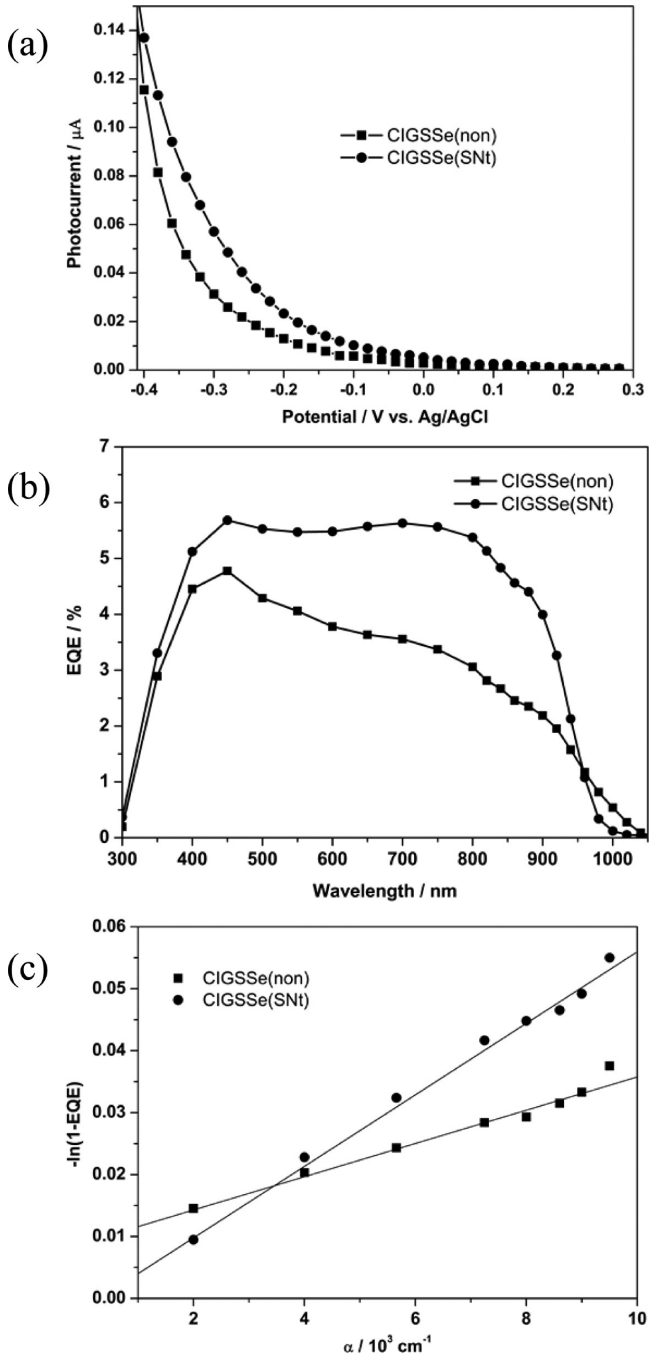

Figure 3. (a) Photocurrent−potential curves of CIGSSe films obtained without and with addition of $NaNO_3$ measured in 0.2 M $Eu(NO_3)_3$ using 550 nm monochromatic light with the lock-in technique. (b) Their EQE spectra measured at −0.4 V vs Ag/AgCl and (c) plot to determine the width of the space charge region (W).

The CIGSSe films were then processed into solar cells with the structure of Al:ZnO/ZnO/CdS/CIGSSe/Mo/glass. Figure 4a and b shows typical photo and dark $J-V$ curves and external quantum efficiency (EQE) spectrum of the solar cells derived

DOI: 10.1021/am507684x
ACS Appl. Mater. Interfaces 2015, 7, 6472−6479

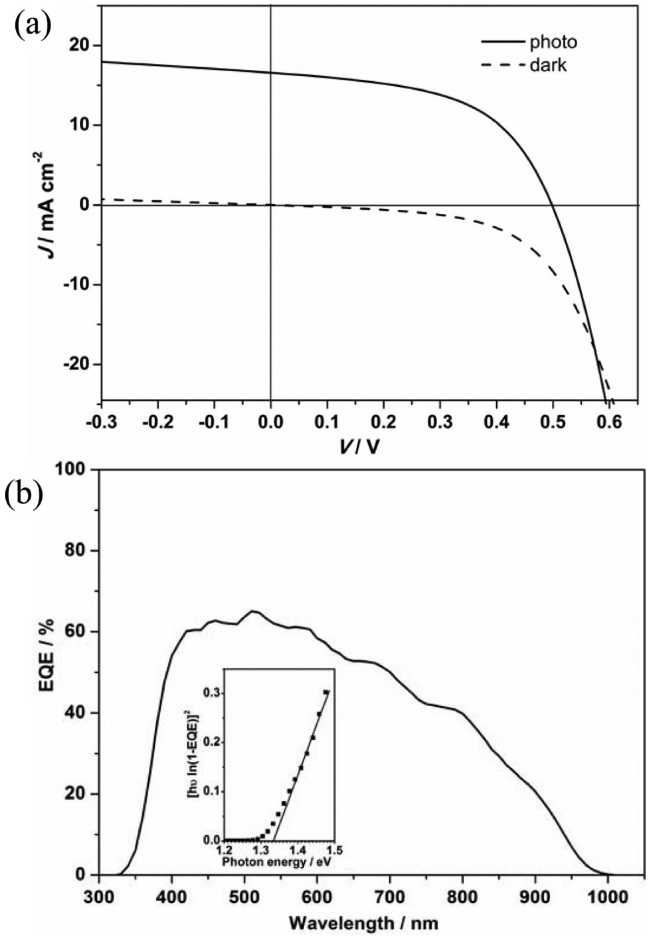

Figure 4. (a) Typical $J-V$ curve and (b) EQE spectrum of a solar cell using a CIGSSe film obtained without addition of $NaNO_3$ (CIGSSe-(non)).

from the CIGSSe(non) film, respectively. Although these $J-V$ curves apparently include poor properties, for example, obvious leakage, high resistance, and crossover behavior between photo and dark curves, an appreciable solar cell property with η of 4.4% was obtained. The band gap energy (E_g) of the CIGSSe absorber was estimated to be 1.33 eV (see inset in Figure 4b). The relatively large E_g compared to the conventional CIGSe with similar Ga content (1.15 eV) indicates the presence of sulfur components in the film, as expected from the above XRD and elemental analyses. In the EQE spectrum, there was a significant drop of the EQE response at a relatively long wavelength region, leading to reduction of short circuit current density (J_{SC} = 17 mA cm^{-2}). This can be attributed to relatively short minority carrier (i.e., electron) diffusion length caused by a highly doped nature of the CIGSSe(non) film (see above). Regarding the open circuit voltage (V_{OC} = 0.50 V), the V_{OC}-deficit value (i.e., $E_g - V_{OC}$ = 0.83 V) of the present device is much larger than that of a highly efficient CIGSe-based device (0.412 V) reported in the literature.[35] Moreover, an appreciable low fill factor (FF = 0.53) and crossover behavior between photo and dark $J-V$ curves indicate that there should be many structural and electrical failures to be improved, such as removal of a high interfacial resistance between the CIGSSe film and Mo substrate[30] and reduction of defects at the CdS-CIGSSe heterojunction.[36]

As shown in Figure 5a, the photo $J-V$ curve of the solar cell based on the CIGSSe(SNt) film showed considerable improve-

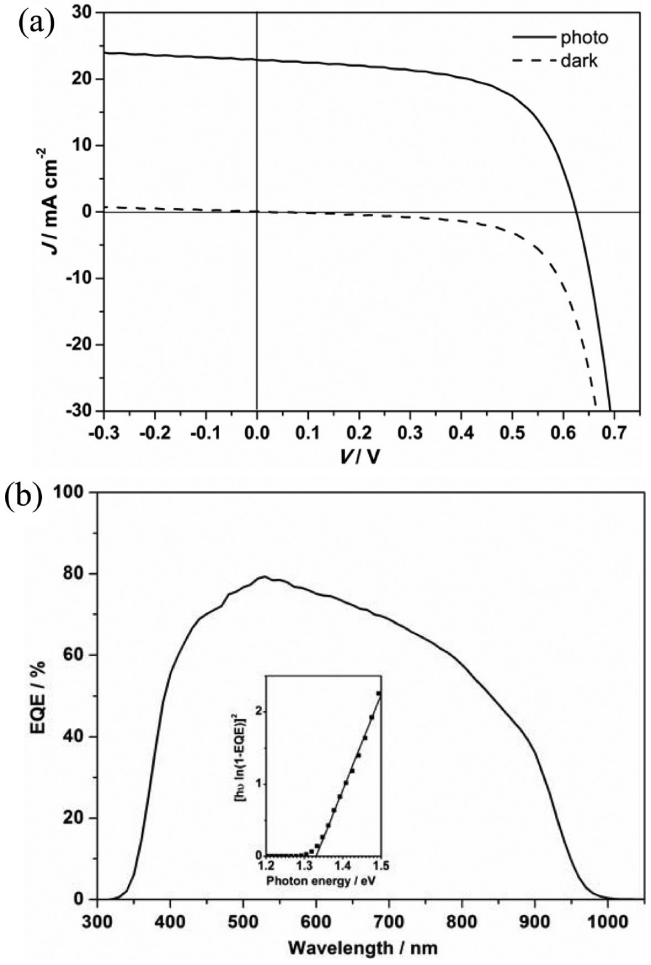

Figure 5. (a) Typical $J-V$ curve and (b) EQE spectrum of solar cell using CIGSSe films obtained with addition of $NaNO_3$ (CIGSSe-(SNt)).

ments of device properties with η, J_{SC}, V_{OC}, and FF of 8.8%, 23 mA cm^{-2}, 0.63 V, and 0.61, respectively. The corresponding EQE spectrum presented in Figure 5b showed a significant improvement in the carrier collection property, especially in the relatively long wavelength region. As mentioned above, successful reduction of majority carrier (hole) density achieved by the addition of $NaNO_3$ during fabrication of the CIGSSe(SNt) film should lead to the observed large increments of J_{SC} compared to the above solar cell based on the CIGSSe(non) film.[37,38] In addition, the thick CIGSSe absorber would also increase the amount of absorbed photons especially in a long wavelength region. Dissapearance of the crossover behavior also indicated improvements of CIGSSe-Mo and CdS-CIGSSe interfaces come from the relatively thin $MoSe_2$ layer and dense CIGSSe film stucture (see Figure 2), respectively, leading to increases in all of the device properties.

In order to optimize the device properties, an MgF_2 antireflection layer was applied to the cell based on CIGSSe-(SNt) film. Table 1 summarized the typical device properties of several MgF_2-coated devices. As expected, J_{SC} values tended to be increased after applying the antireflection in all the cases. One of the devices reached the maximum conversion efficiency

DOI: 10.1021/am507684x
ACS Appl. Mater. Interfaces 2015, 7, 6472−6479

Table 1. Statistical data of J_{SC}, V_{OC}, FF, and η of the MgF_2-Coated Devices Based on CIGSSe(SNt) Absorber

no.	J_{SC} (mA cm^{-2})	V_{OC} (V)	FF	η (%)
1	24	0.62	0.62	9.2
2	25	0.62	0.61	9.4
3	26	0.62	0.63	10.1
4	28	0.64	0.60	10.7
5	25	0.61	0.60	9.0
6	25	0.62	0.63	10.0
7	25	0.61	0.61	9.2

of 10.7% with J_{SC} of 28 mA cm^{-2}. It should be noted that the optimal cell without applying the MgF_2 coating might have a high J_{SC} value of more than 23 mA cm^{-2} though we did not have device properties of the cell without MgF_2. To the best of our knowledge, this efficiency is one of the highest reported for chalcopyrite solar cells fabricated by using a nontoxic aqueous precursor route, and it is comparable to a recent report showing 10.5%-efficient device based on the spray-pyrolysis method.[39] The devices properties were relatively stable with no observed appreciable degradation upon prolonged exposure in air and/or under repetitive measurements.

SIMS profiles of thus-obtained solar cells based on CIGSSe(non) and CIGSSe(SNt) are shown in Figure 6a and 6b, respectively. An obvious gradient of the sodium content along the thickness direction was observed in the CIGSSe-(non)-based sample, where appreciable amounts of sodium comparable to those in a typical CIGSe film (see above) were included in the near back contact of the absorber (~3 × 10^{20}

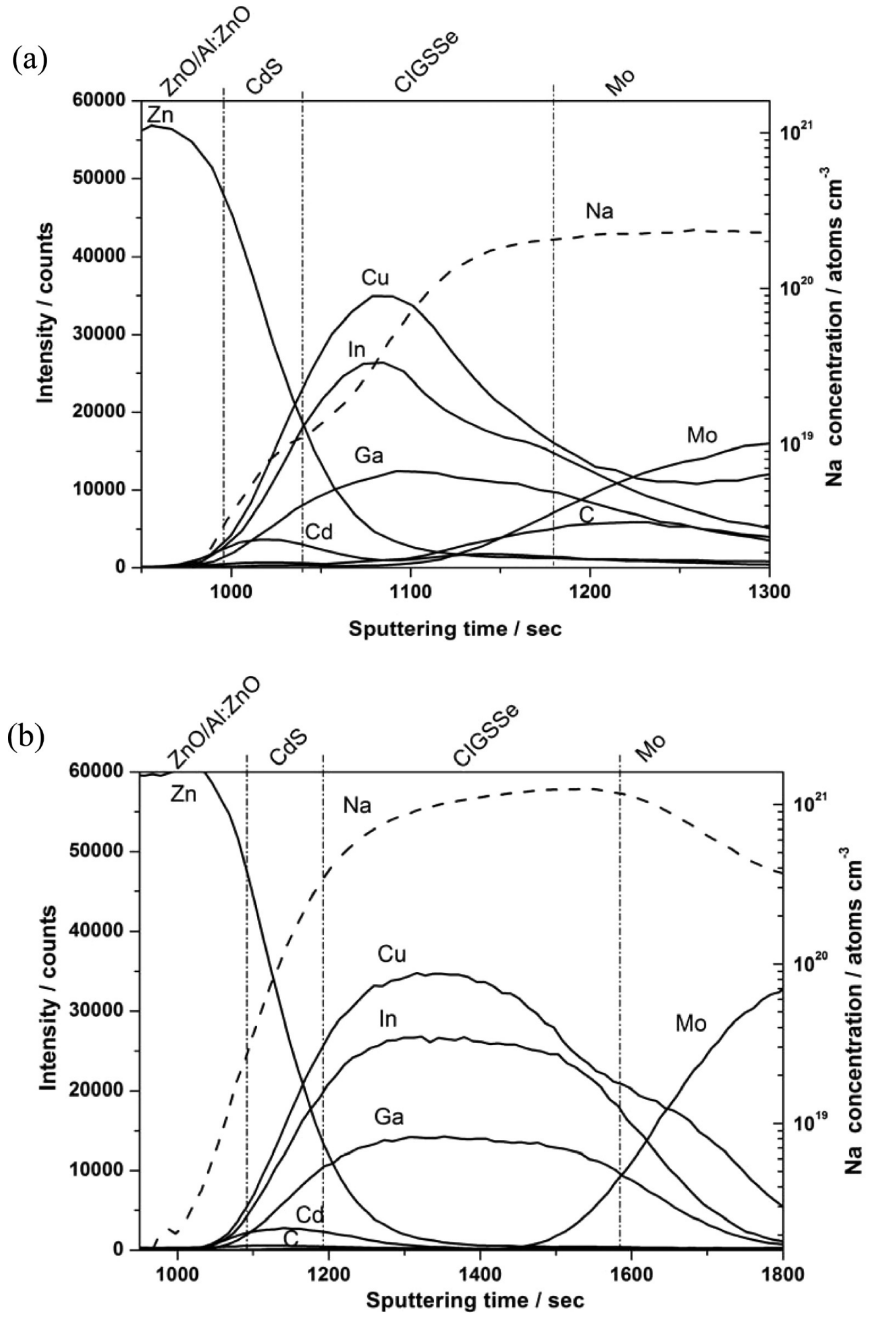

Figure 6. SIMS profiles of the solar cells using (a) CIGSSe(non) and (b) CIGSSe(SNt).

DOI: 10.1021/am507684x
ACS Appl. Mater. Interfaces 2015, 7, 6472−6479

atoms cm^{-3}). This sodium-gradient-profile suggests that the sodium was slowly diffused from the soda-lime glass during the present selenization process. As expected, much larger amount of sodium with homogeneous distribution was observed for the CIGSSe(SNt)-based sample ($\sim 1-1.5 \times 10^{21}$ atoms cm^{-3}), though the number of atoms was somewhat smaller than that estimated from the Na/(In + Ga) composition (0.3) of the spray solution (3.6×10^{21} atoms cm^{-3}). Another point worth noting is that an appreciable amount of carbon was existed at the interface between CIGSSe(non) and Mo-back contact, indicating an incomplete decomposition of the remaining organic compound on the film both during the spray deposition as well as the selenization process. On the other hand, the CIGSSe(SNt) film contained negligible amount of carbon, implying that addition of $NaNO_3$ is beneficial for reduction of carbon impurity in the final CIGSSe film.

The above-described PEC analyses indicated that an appreciable decrease in N_a of the CIGSSe film could be achieved by dissolving $NaNO_3$ in the spray solution. Scanning spreading resistance microscopy (SSRM) measurements of the devices derived from the CIGSSe(non) and CIGSSe(SNt) films also supported these findings; i.e., the CIGSSe(SNt) absorber exhibited higher resistance than that of the CIGSSe-(non) absorber (see Supporting Information Figure S3). The sodium-doping (or loading) effect obtained in this study seems to be opposite to the commonly reported effect of sodium because the addition of sodium usually resulted in increment of N_a.[17,20] Most of the reported CIGSe absorbers usually had a suitable acceptor density for solar cell application (in the order of $10^{15}-10^{16}$ cm^{-3}) even without any intentional sodium addition. A similar behavior of the reduction of N_a was observed by applying NaCl treatment to nanoink-based CIGSSe absorbers, though there was no detailed explanation for this observation.[15] Therefore, further study is required to clarify the exact role in sodium to the electronic properties of our spray-pyrolysis-based CIGSSe samples.

4. CONCLUSION

In this study, we investigated fabrication of CIGSSe thin films by selenization of CIGS precursor films obtained by spray pyrolysis. We showed that addition of $NaNO_3$ to the precursor solution effectively promotes enhancement of the crystallization process of the precursor film during spray-pyrolysis deposition as well as the final CIGSSe film during the selenization process. The sodium-added CIGSSe film had an interconnected morphology of grains with relatively dense structure compared to that of the CIGSSe film obtained without addition of sodium. The solar cell based on the sodium-modified film showed a maximum conversion efficiency of 10.7% after applying an antireflection coating. The addition of sodium to the CIGSSe absorber was found to be effective for reducing the majority carrier concentration in the film when the highly doped bare CIGSSe absorber film was used.

■ ASSOCIATED CONTENT

Supporting Information

Surface and cross-sectional SEM images of as-sprayed films, photoelectrochemical estimation of acceptor density of coevaporated CIGSe film, and resistivity profile of the devices measured with scanning spreading resistance microscopy. This material is available free of charge via the Internet at http://pubs.acs.org.

■ AUTHOR INFORMATION

Corresponding Author

*E-mail: sikeda@chem.es.osaka-u.ac.jp.

Notes

The authors declare no competing financial interest.

■ ACKNOWLEDGMENTS

S.I. acknowledges for financial support by a Grant-in-Aid for Scientific Research on Innovative Areas (All Nippon Artificial Photosynthesis Project for Living Earth) from MEXT Japan. Dr. Takeshi Yamauchi and Mr. Tatsuya Nakao (Analysis Simulation Center, Asahi Kasei Corporation) are gratefully acknowledged for their analyses in SIMS and SSRM measurements.

■ REFERENCES

(1) Jackson, P.; Hariskos, D.; Wuerz, R.; Kiowski, O.; Bauer, A.; Friedlmeier, T. M.; Powalla, M. Properties of $Cu(In,Ga)Se_2$ with new record efficiencyies up to 21.7%. *Phys. Status Solidi RRL* **2014**, *9* (1), 28−31 DOI: 10.1002/pssr.201409520.

(2) Green, M. A.; Emery, K.; Hishikawa, Y.; Warta, W.; Dunlop, E. D. Solar Cell Efficiency Tables (Version 43). *Prog. Photovolt: Res. Appl.* **2014**, *22*, 1−9.

(3) Reinhard, P.; Buecheler, S.; Tiwari, A. N. Technological Status of $Cu(In,Ga)(Se,S)_2$-Based Photovoltaics. *Sol. Energy Mater. Sol. Cells* **2013**, *119*, 287−290.

(4) Kushiya, K. CIS-based Thin-Film PV Technology in Solar Frontier K.K. *Sol. Energy Mater. Sol. Cells* **2014**, *122*, 309−313.

(5) Siebentritt, S.; Gütay, L.; Regesch, D.; Aida, Y.; Deprédurand, V. Why Do We Make $Cu(In,Ga)Se_2$ Solar Cells Non-Stoichiometric? *Sol. Energy Mater. Sol. Cells* **2013**, *119*, 18−25.

(6) Yan, Y.; Noufi, R.; Al-Jassim, M. M. Grain-Boundary Physics in Polycrystalline $CuInSe_2$ Revisited: Experiment and Theory. *Phys. Rev. Lett.* **2006**, *96*, No. 205501.

(7) Yan, Y.; Jiang, C.-S.; Noufi, R.; Wei, S. H.; Moutinho, H. R.; Al-Jassim, M. M. Electrically Benign Behavior of Grain Boundaries in Polycrystalline $CuInSe_2$ Films. *Phys. Rev. Lett.* **2007**, *99*, No. 235504.

(8) Todorov, T.; Mitzi, D. B. Direct Liquid Coating of Chalcopyrite Light-Absorbing Layers for Photovoltaic Devices. *Eur. J. Inorg. Chem.* **2010**, *2010*, 17−28.

(9) Hibberd, C. J.; Chassaing, E.; Liu, W.; Mitzi, D. B.; Lincot, D.; Tiwari, A. N. Non-Vacuum Methods for Formation of $Cu(In,Ga)(Se,S)_2$ Thin Film Photovoltaic Absorbers. *Prog. Photovolt: Res. Appl.* **2010**, *18*, 434−452.

(10) Eslamian, M. Spray-on Thin Film PV Solar Cells: Advances, Potentials and Challenges. *Coatings* **2014**, *4*, 60−84.

(11) Ikeda, S.; Nonogaki, M.; Septina, W.; Gunawan, G.; Harada, T.; Matsumura, M. Fabrication of $CuInS_2$ and $Cu(In,Ga)S_2$ Thin Films by a Facile Spray Pyrolysis and Their Photovoltaic and Photoelectrochemical Properties. *Catal. Sci. Technol.* **2013**, *3*, 1849−1854.

(12) Ho, J. C. W.; Zhang, T.; Lee, K. K.; Batabyal, S. K.; Tok, A. I. Y.; Wong, L. H. Spray Pyrolysis of $CuIn(S,Se)_2$ Solar Cells with 5.9% Efficiency: A Method to Prevent Mo Oxidation in Ambient Atmosphere. *ACS Appl. Mater. Interface* **2014**, *6*, 6638−6643.

(13) Shirakata, S.; Murakami, T.; Kariya, T.; Isomura, S. Preparation of $CuInSe_2$ Thin Films by Chemical Spray Pyrolysis. *Jpn. J. Appl. Phys.* **1996**, *35* (1R), 191−199.

(14) Shirakata, S.; Kannaka, Y.; Hasegawa, H.; Kariya, T.; Isomura, S. Properties of $Cu(In,Ga)$ Se_2 Thin Films Prepared by Chemical Spray Pyrolysis. *Jpn. J. Appl. Phys.* **1999**, *38*, 4997−5002.

(15) Guo, Q.; Ford, G. M.; Agrawal, R.; Hillhouse, H. W. Ink Formulation and Low-Temperature Incorporation of Sodium to Yield 12% efficient $Cu(In,Ga)(S,Se)_2$ Solar Cells from Sulfide Nanocrystal Inks. *Prog. Photovolt: Res. Appl.* **2013**, *21*, 64−71.

(16) Chirilă, A.; Reinhard, P.; Pianezzi, F.; Bloesch, P.; Uhl, A. R.; Fella, C.; Kranz, L.; Keller, D.; Gretener, C.; Hagendorfer, H.; Jaeger, D.; Erni, R.; Nishiwaki, S.; Buecheler, S.; Tiwari, A. N. Potassium-

DOI: 10.1021/am507684x
ACS Appl. Mater. Interfaces 2015, 7, 6472−6479

Induced Surface Modification of Cu(In,Ga)Se_2 Thin Films for High-Efficiency Solar Cells. *Nat. Mater.* **2013**, *12*, 1107−1111.
(17) Nakada, T.; Iga, D.; Ohbo, H.; Kunioka, A. Effects of Sodium on Cu(In,Ga)Se_2-Based Thin Films and Solar Cells. *Jpn. J. Appl. Phys.* **1997**, *36*, 732−737.
(18) Blösch, P.; Nishiwaki, S.; Kranz, L.; Fella, C.; Pianezzi, F.; Jäger, T.; Adelhelm, C.; Franzke, E.; Buecheler, S.; Tiwari, A. Sodium-Doped Molybdenum Back Contact Designs for Cu(In,Ga)Se_2 Solar Cells. *Sol. Energy Mater. Sol. Cells* **2014**, *124*, 10−16.
(19) Rudigier, E.; Pietzker, C.; Wimbor, M.; Luck, I.; Klaer, J.; Scheer, R.; Barcones, B.; Colin, T. J.; Alvarez-Garcia, J.; Perez-Rodriguez, A.; Romano-Rodriguez, A. Real-Time Investigations of The Influence of Sodium on The Properties of Cu-Poor Prepared $CuInS_2$ Thin Films. *Thin Solid Films* **2003**, *431−432*, 110−115.
(20) Kronik, L.; Cahen, D.; Schock, H. W. Effects of Sodium on Polycrystalline Cu(In,Ga)Se_2 and Its Solar Cell Performance. *Adv. Mater.* **1998**, *10*, 31−36.
(21) Scragg, J. J.; Dale, P. J.; Peter, L. M. Towards Sustainable Materials for Solar Energy Conversion: Preparation and Photoelectrochemical Characterization of Cu_2ZnSnS_4. *Electrochem. Commun.* **2008**, *10*, 639−642.
(22) Lee, S. M.; Ikeda, S.; Otsuka, Y.; Septina, W.; Harada, T.; Matsumura, M. Homogeneous Electrochemical Deposition of In on a Cu-Covered Mo Substrate for Fabrication of Efficient Solar Cells with a $CuInS_2$ Photoabsorber. *Electrochim. Acta* **2012**, *79*, 189−196.
(23) Peter, L. M. Dynamic Aspects of Semiconductor Photoelectrochemistry. *Chem. Rev.* **1990**, *90*, 753−769.
(24) Wei, S.-H.; Zhang, S. B.; Zunger, A. Effects of Ga Addition to $CuInSe_2$ on Its Electronic, Structural, and Defect Properties. *Appl. Phys. Lett.* **1998**, *72*, 3199−3201.
(25) Cai, Y.; Ho, J. C. W.; Batabyal, S. K.; Liu, W.; Sun, Y.; Mhaisalkar, S. G.; Wong, L. H. Nanoparticle-Induced Grain Growth of Carbon-Free Solution-Processed $CuIn(S,Se)_2$ Solar Cell with 6% Efficiency. *ACS Appl. Mater. Interfaces* **2013**, *5*, 1533−1537.
(26) Albin, D.; Tuttle, J.; Noufi, R. The Formation of Large-Grain $CuInSe_2$ Films by Selenization by High-Rate Se Transport Under Moderate Vacuum Conditions. *J. Electron. Mater.* **1995**, *24*, 351−357.
(27) Braunger, D.; Hariskos, D.; Bilger, G.; Rau, U.; Schock, H. W. Influence of Sodium on The Growth of Polycrystalline Cu(In,Ga)Se_2 Thin Films. *Thin Solid Films* **2000**, *361−362*, 161−166.
(28) Mansfield, L. M.; Repins, I. L.; Glynn, S.; Carducci, M. D.; Honecker, D. M.; Pankow, J. W.; Young, M. R.; DeHart, C.; Sundaramoorthy, R.; Beall, C. L.; To, B. *Proc. Photovoltaic Specialists Conference (PVSC), 2011 37th IEEE* **2011**, 003636−003641.
(29) Minoura, S.; Kodera, K.; Maekawa, T.; Miyazaki, K.; Niki, S.; Fujiwara, H. Dielectric Function of Cu(In,Ga)Se_2-Based Polycrystalline Materials. *J. Appl. Phys.* **2013**, *113*, No. 063505.
(30) Eisenbarth, T.; Unold, T.; Caballero, R.; Kaufmann, C. A.; Schock, H.-W. Interpretation of Admittance, Capacitance-Voltage, and Current-Voltage Signatures in Cu(In,Ga)Se_2 Thin Film Solar Cells. *J. Appl. Phys.* **2010**, *107*, No. 034509.
(31) Dullweber, T.; Lundberg, O.; Malmström, J.; Bodegård, M.; Stolt, L.; Rau, U.; Schock, H. W.; Werner, J. H. Back Surface Band Gap Gradings in Cu(In,Ga)Se_2 Solar Cells. *Thin Solid Films* **2011**, *387*, 11−13.
(32) Werner, J. H.; Mattheis, J.; Rau, U. Efficiency Limitations of Polycrystalline Thin Film Solar Cells: Case of Cu(In,Ga)Se_2. *Thin Solid Films* **2005**, *480−481*, 399−409.
(33) Bhattacharya, R. N.; Hiltner, J. F.; Batchelor, W.; Contreras, M. A.; Noufi, R. N.; Sites, J. R. 15.4% $CuIn_{1-x}Ga_xSe_2$-Based Photovoltaic Cells From Solution-Based Precursor Films. *Thin Solid Films* **2000**, *361*, 396−399.
(34) Negami, T.; Satoh, T.; Hashimoto, Y.; Nishiwaki, S.; Shimakawa, S.; Hayashi, S. Large-Area CIGS Absorbers Prepared by Physical Vapor Deposition. *Sol. Energy Mater. Sol. Cells* **2001**, *67*, 1−9.
(35) Jackson, P.; Hariskos, D.; Lotter, E.; Paetel, S.; Wuerz, R.; Menner, R.; Wischmann, W.; Powalla, M. New World Record Efficiency for Cu(In,Ga)Se_2 Thin-Film Solar Cells Beyond 20%. *Prog. Photovolt: Res. Appl.* **2011**, *19*, 894−897.
(36) Burgelman, M.; Engelhardt, F.; Guillemoles, J. F.; Herberholz, R.; Igalson, M.; Klenk, R.; Lampert, M.; Meyer, T.; Nadenau, V.; Niemegeers, A.; Parisi, J.; Rau, U.; Schock, H. W.; Schmitt, M.; Seifert, O.; Walter, T.; Zott, S. Defects in Cu(In,Ga)Se_2 Semiconductors and Their Role in The Device Performance of Thin-Film Solar Cells. *Prog. Photovolt: Res. Appl.* **1997**, *5*, 121−130.
(37) Nichterwitz, M.; Caballero, R.; Kaufmann, C. A.; Schock, H.-W.; Unold, T. Generation-Dependent Charge Carrier Transport in Cu(In,Ga)Se_2/CdS/ZnO Thin-Film Solar-Cells. *J. Appl. Phys.* **2013**, *113*, No. 044515.
(38) Nichterwitz, M.; Unold, T. Numerical Simulation of Cross Section Electron-Beam Induced Current in Thin-Film Solar-Cells for Low and High Injection Conditions. *J. Appl. Phys.* **2013**, *114*, No. 134504.
(39) Hossain, M. A.; Tianliang, Z.; Keat, L. K.; Xianglin, L.; Prabhakar, R. R.; Batabyal, S. K.; Mhaisalkar, S. G.; Wong, L. H. Synthesis of Cu(In,Ga)$(S,Se)_2$ Thin Films using an Aqueous Spray-Pyrolysis Approach, and Their Solar Cell Efficiency of 10.5%. *J. Mater. Chem. A* **2015**, *3* (8), 4147−4154.

DOI: 10.1021/am507684x
ACS Appl. Mater. Interfaces 2015, 7, 6472−6479